Environmental Science & Technology

Article

pubs.acs.org/est

Iron and Arsenic Speciation and Distribution in Organic Flocs from Streambeds of an Arsenic-Enriched Peatland

Laurel K. ThomasArrigo,[†] Christian Mikutta,*[,†] James Byrne,[‡] Kurt Barmettler,[†] Andreas Kappler,[‡] and Ruben Kretzschmar[†]

[†]Soil Chemistry Group, Institute of Biogeochemistry and Pollutant Dynamics, Department of Environmental Systems Science, CHN, ETH Zurich, 8092 Zurich, Switzerland

[‡]Geomicrobiology Group, Centre for Applied Geosciences (ZAG), University of Tübingen, Sigwartstrasse 10, 72076, Tübingen, Germany

Supporting Information

ABSTRACT: Iron-rich organic flocs are frequently observed in surface waters of wetlands and show a high affinity for trace metal(loid)s. To date, spectroscopic speciation analyses of Fe and trace elements in these mineral-organic matter (OM) associations are missing. In this study, we investigated the speciation and distribution of Fe and As in flocs collected from low-flow streams (pH 5.3−6.3) of the naturally As-enriched peatland *Gola di Lago* (Switzerland) using ^{57}Fe Mössbauer spectroscopy and synchrotron X-ray techniques. The flocs were rich in acid carbohydrates and contained up to 22.1 wt % Fe, 34.9 wt % C, and 2620 mg/kg As. Mössbauer analyses revealed small quantities (<5%) of Fe(II) and Fe(III)-OM complexes and the predominance of ferrihydrite (~$Fe_5HO_8{\cdot}4H_2O$, 51−59%) and lepidocrocite (γ-FeOOH, 34−46%). The latter was not observed by synchrotron X-ray diffraction, implying a coherent scattering domain size of <10 nm. Iron X-ray absorption spectroscopy (XAS) confirmed the Mössbauer results, and bulk As XAS indicated the prevalence of arsenate (71−84%) in the flocs. Shell-fit analyses showed that As was entirely sorbed to Fe(III)-(oxyhydr)oxides and that both arsenate and arsenite exclusively formed monodentate-binuclear ("bridging") complexes (R_{As-Fe} = 3.31−3.34 Å). Microfocused X-ray fluorescence spectrometry documented a strong correlation between As and Fe in the flocs. These analyses also revealed intense As hotspots coinciding with abundant freshwater green algae (*Closterium* spp.). Microfocused As X-ray absorption near-edge structure spectra collected at algae-specific points identified up to 29% As(III), which, in combination with ~5% As(III) detected at Fe-rich points, suggests As(V) bioreduction in the algae. Our findings imply that floc (bio)organics serve primarily as nucleation sites for the precipitation of nanocrystalline Fe(III)-(oxyhydr)oxides, rendering flocs effective sorbents for trace metal(loid)s. Thus, Fe-rich freshwater flocs likely play a pivotal role for the speciation and cycling of trace elements in wetlands.

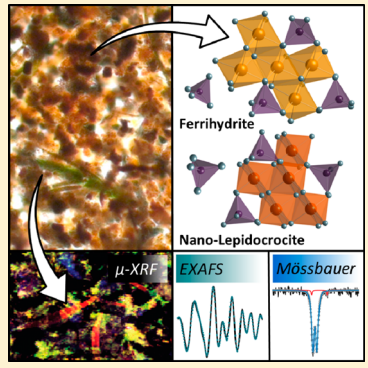

INTRODUCTION

In freshwater ecosystems like lakes and wetlands, associations of mineral phases, microorganisms, and organic detritus are intricately sustained in matrices of microbial exopolymeric substances (EPS). These associations, termed "flocs", are frequently observed as suspended or settled, micro- to millimeter-sized particulate matter[1−3] and exhibit a high sorption capacity for trace elements. As a result, trace element concentrations in flocs can be significantly higher than those of the corresponding surficial bed sediments.[1,4,5] For example, Elliot et al.[4] reported floc metal(loid) enrichment factors (EF = c_{floc}/c_{bed}) of up to 55. Continually interacting with their aquatic surroundings,[3] flocs are subject to geochemical changes in the water column and can be mobilized by storm or flooding events. The mobility of flocs depends on their physicochemical characteristics (e.g., size, porosity, content of microbial biomass) and the prevailing water flow conditions.[3,6,7] Wetlands tend to offer low-flow regimes with relatively low shear stresses, facilitating biostabilization of floc material in the water column.[6] Contrastingly, high-flow velocity events like storms can greatly affect floc mobility controls[7] and, in turn, floc metal(loid) retention. Plach et al.[1] recorded significant concentration increases of Ag (from 0.01 to 7.35 μmol/g) and Cu (from 0.60 to 1.45 μmol/g) in flocs following storm events, as well as surges in crystalline Fe/Mn-(oxyhydr)oxide-associated metal(loid)s in storm-sampled flocs, likely due to mineral phase contributions from mobilized bed sediments. Based on sequential extractions, trace elements in flocs have been shown to primarily reside in the "amorphous" and "crystalline" Fe/Mn-(oxyhydr)oxide fractions,[1,4] whose composition may change over time. Elliot and Warren[8] observed seasonal shifts in microbial communities of lacustrine flocs which induced changes in Fe mineralogy from primarily amorphous Fe(III) phases (summer) to more crystalline Fe(III) and Fe(II) phases (winter). These changes were

Received: July 22, 2014
Revised: September 24, 2014
Accepted: October 1, 2014
Published: October 27, 2014

ACS Publications © 2014 American Chemical Society

accompanied by decreases in floc Cd and Pb concentrations.[8] Although Fe/Mn mineralogy exerts an important control on trace element binding in flocs, the identity of the mineral phases involved and their properties remain largely elusive. This information, however, is essential to understanding trace element cycling in freshwater environments. Recently, Sundman et al.[9] investigated the speciation of Fe in dissolved organic matter (OM) from a forest catchment stream (8.4 μM Fe). Based on shell fits of extended X-ray absorption fine structure (EXAFS) spectra, the OM contained significant amounts of organically complexed, mononuclear Fe(III) species and Fe(III)-(oxyhydr)oxides which they interpreted as ferrihydrite (e.g., $\sim Fe_5HO_8{\cdot}4H_2O$).[10]

The naturally As-enriched ($\leq$1800 mg As/kg)[11] minerotrophic peatland *Gola di Lago* (Switzerland) is characterized by abundant Fe-rich flocs in surface waters of the permanent streams draining the peatland (Supporting Information (SI) Figure S1). Their proximity to a recognized As sink[11,12] provides ideal circumstances to investigate the speciation of Fe and As in freshwater flocs. Previous X-ray absorption spectroscopy (XAS) and microfocused X-ray fluorescence (μ-XRF) spectrometry studies of *Gola di Lago* peat cores showed that in deep anoxic peat layers, As(III) was homogeneously distributed and mainly coordinated to 2−3 S atoms with interatomic As−S distances of ~2.26 Å.[11,13] These results implied the covalent binding of As(III) to sulfhydryl groups of peat OM (As(III)-S_{org}), which can proceed by sorption of arsenite to S-rich OM.[14] In contrast, 10−50 μm-sized realgar (α-As_4S_4) was identified as a major As species in near-surface peat layers (<40 cm).[11,13] Since both As(III)-S_{org} complexes and realgar have been shown to oxidize slowly under ambient conditions with half-life times of 312 and 215 days, respectively,[15] S-associated As could be an important As species in the flocs. On the other hand, high OM contents in flocs may facilitate the formation of ternary arsenite and arsenate complexes, in which mono- or oligomeric Fe(III) species serve as bridges between organic ligands and As.[16−18] Moreover, arsenite has been shown to readily react with hydroxylic/phenolic groups of peat OM under reducing conditions,[16] which may imply that arsenite is stabilized by floc OM in suboxic or oxic waters. Alternatively, As may be immobilized by Fe(III)-(oxyhydr)oxides formed by phototrophic Fe(II)-oxidizing bacteria[19] or mixed-valence Fe minerals like green rusts ($[Fe(II)_{1-n}Fe(III)_n(OH)_2]^{n+}(CO_3,Cl,SO_4)^{n-}$) under sub- and anoxic conditions,[20] or be entirely sequestered by Fe(III)-(oxyhydr)oxides at higher O_2 fugacities.[21] Because freshwater flocs comprise multiple potential sorbents for As, detailed spectroscopic investigations are required to determine the partitioning of As between inorganic and organic floc constituents and to infer its oxidation state and local (<5 Å) coordination environment. Therefore, we used ^{57}Fe Mössbauer spectroscopy and synchrotron techniques (XAS, μ-XRF spectrometry, X-ray diffraction) to explore the dominating Fe species, the bulk and microscale speciation and distribution of As, and the importance of OM for As retention in freshwater flocs collected from streambeds of the *Gola di Lago* peatland.

MATERIALS AND METHODS

Study Site and Sample Characterization. Iron-rich flocs (n = 14) were collected in October 2012 from 10 to 30 cm thick, loosely consolidated floc layers at the bottom of low-flow surface streams of the naturally As-enriched minerotrophic peatland *Gola di Lago* (canton Ticino, Switzerland)[12] (SI Figure S1). The flocs were collected in beakers without disturbing the underlying peat, immediately flash-frozen with liquid N_2, transported on dry ice to the laboratory, and freeze-dried. They were then sieved (<500 μm), homogenized with a mortar and pestle, and stored anoxically (<10 ppm (v/v) O_2). Additional sample material was collected in vials and stored in darkness at 4 °C for microscale analyses.

Surface waters at floc sampling locations were analyzed on-site for standard geochemical parameters such as E_h, pH, T (Metrohm 826), dissolved O_2 (Hach HQ30D), and electrical conductivity (WTW 315i). Dissolved organic C (DOC) concentrations in 0.45-μm filtered water samples were determined with a Dimatoc 2000 TOC analyzer (Dimatec), and total element concentrations were determined in 0.2-μm filtrates using inductively coupled plasma-mass spectrometry (ICP-MS, 7500ce, Agilent) and inductively coupled plasma-optical emission spectrometry (ICP-OES, Vista-MPX, Varian). Dissolved Fe(II) could not be detected ([Fe(II)] <10 μg/L) in the streams by spectrophotometry (Nanocolor test 1−36, Nanocolor 500 D, Macherey-Nagel).

Total element contents in the flocs were assessed with ICP-MS or ICP-OES after microwave-assisted acid digestion (MLS turboWave), and total C and N contents were determined with an elemental analyzer (CHNS-932, LECO). Attenuated total reflectance Fourier-transform infrared (ATR-FTIR) spectroscopy was used to characterize functional groups of the OM fraction. The spectra were recorded with a resolution of 1/cm on a Bio-Rad FTS 575C spectrometer equipped with a Harrick Meridian diamond single reflection SplitPea ATR unit.

Nonfreeze-dried floc material was imaged by light microscopy (Zeiss Axioskop 40). Flocs were plated on glass slides and dried at room temperature (24 ± 1 °C). For imaging of cell DNA, additional samples were stained with 4′,6-diamidino-2-phenylindole (DAPI) and analyzed by fluorescence microscopy (Leica DM6000 B).

^{57}Iron Mössbauer Spectroscopy. Mössbauer spectra of selected samples (n = 8) were obtained with a ^{57}Co/Rh γ-radiation source with an activity of ~35 mCi vibrated in constant acceleration mode in a standard setup (WissEl, Wissenschaftliche Elektronik GmbH). Freeze-dried sample material (30−60 mg) was loaded into Plexiglas sample holders (~1 cm^2) under anoxic conditions and mounted in transmission geometry. Sample temperatures were varied with a closed-cycle cryostat (SHI-850-I, Janis Research Co.), whereas the ^{57}Co/Rh source remained at room temperature. Spectra were collected at 295 and 5 K, and analyzed using the Recoil software (University of Ottawa, Canada) and Voigt-based fitting routines. The spectra were calibrated against α-$^{57}Fe^0$ at 295 K and center shifts (CS) are quoted relative to this. For all samples the half width at half-maximum was fixed to 0.122 mm/s; the value of the inner line broadening of the calibration foil at 295 K.

Synchrotron Measurements. The mineralogical composition of the flocs was investigated by synchrotron X-ray diffraction (SXRD). Homogenized sample powders were loaded into 1 mm o.d. borosilicate glass capillaries under anoxic conditions and analyzed at beamline X04SA[22] of the Swiss Lightsource (SLS, Villigen, Switzerland). The measurements were performed in transmission mode and Debye−Scherrer geometry using a MYTHEN-II Si strip detector and an incident X-ray energy of 20 keV (λ = 0.6199 Å).

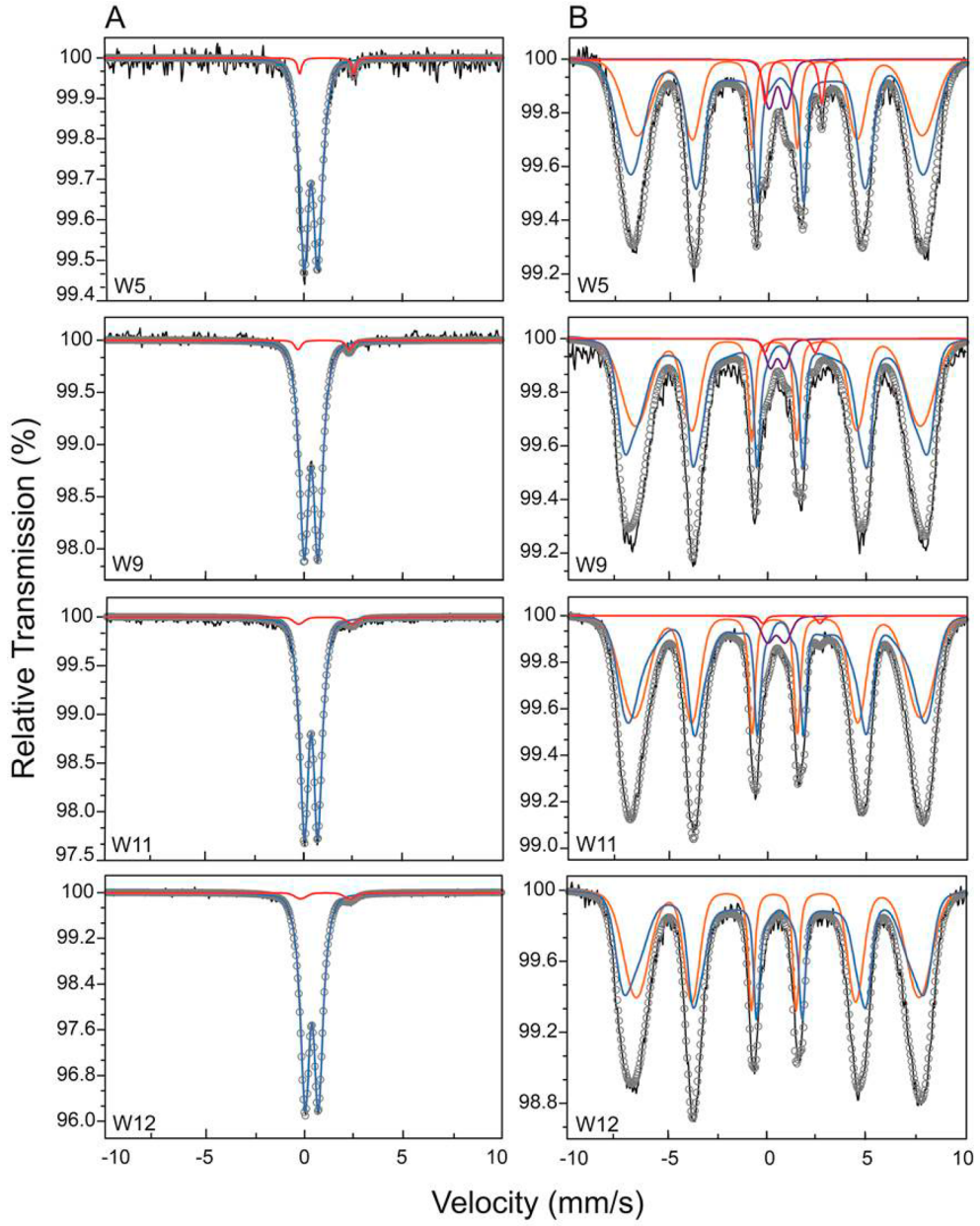

Figure 1. Mössbauer spectra of selected floc samples recorded at (A) 295 K and (B) 5 K. In all graphs, black lines denote experimental data and circles represent the model fit sum. In (A) blue and red lines refer to the paramagnetic Fe(III) and Fe(II) doublet(s), respectively. In (B) the color code of the fit components is as follows: blue is ferrihydrite (Fe(III)-S1), orange is lepidocrocite (Fe(III)-S2), purple denotes Fe(III)-OM complexes (Fe(III)-D1), and red is adsorbed Fe(II) (Fe(II)-D2). The corresponding Mössbauer parameters are summarized in Table 1. Additional sample spectra recorded at 5 and 295 K are shown in SI Figure S7, and fit parameters of the 295-K spectra are reported in SI Table S3.

Selected samples were also analyzed by bulk Fe K-edge (7112 eV) and As K-edge (11867 eV) X-ray absorption near-edge structure (XANES) and EXAFS spectroscopy at the XAFS beamline of ELETTRA (Trieste, Italy) (Fe) and beamline BM23 of the European Synchrotron Radiation Facility (ESRF, Grenoble, France) (As). Additional samples were analyzed by μ-XRF spectrometry and As μ-XAS at beamline 13-ID-E of the Advanced Photon Source (APS, Argonne, IL). Details on these measurements, data reduction, and analysis are provided in the SI.

RESULTS AND DISCUSSION

Study Site and Sample Characterization. In surface water samples, temperatures were measured between 9.9 and 13.6 °C ($\bar{x}$ = 11.9). The pH was 5.3–6.3 ($\bar{x}$ = 5.9) and the redox potential ranged from −188 to 260 mV ($\bar{x}$ = 11.3). Dissolved O_2 concentrations were well below saturation (1.6–7.6 mg/L, $\bar{x}$ = 3.5), and electrical conductivity values varied between 116 and 420 μS/cm ($\bar{x}$ = 184). Measured DOC concentrations were 5.9–25.9 mg/L ($\bar{x}$ = 9.5), and concentrations of dissolved As, Fe, and S were 0.4–7.6, 50.9–1040, and 749–2240 μg/L, respectively (SI Table S1).

Light microscopy analyses of the flocs revealed micrometer-sized aggregates with highly heterogeneous compositions in terms of OM and mineral content (SI Figure S2). The flocs were interspersed with microbial cells (SI Figure S3), and contained 21.4–34.9 wt % C, 4.9–22.1 wt % Fe, 0.50–1.85 wt % N, and 0.37–0.64 wt % S (SI Table S1). Consistent with

Table 1. Mössbauer Parameters of Floc Samples Measured at 5 K

sample	species	CS[a] (mm/s)	ΔE_Q[b] (mm/s)	ϵ[c] (mm/s)	<|H|>[d] (T)	population[e] (%)	χ^{2f}
W1	Fe(III)-S1[g]	0.52		−0.11	42.3	55.7 ± 3.1	0.62
	Fe(III)-S2	0.44		0.10	45.5	37.8 ± 3.1	
	Fe(III)-D1	0.45	0.97			3.9 ± 0.9	
	Fe(II)-D2	1.26	2.77			2.7 ± 0.6	
W5	Fe(III)-S1	0.50		−0.09	41.7	58.6 ± 3.2	1.04
	Fe(III)-S2	0.43		0.13	44.8	34.3 ± 3.2	
	Fe(III)-D1	0.45	0.89			4.5 ± 1.2	
	Fe(II)-D2	1.25	2.88			2.5 ± 0.5	
W7	Fe(III)-S1	0.51		−0.11	42.3	56.4 ± 2.9	0.74
	Fe(III)-S2	0.41		0.08	46.1	37.9 ± 2.9	
	Fe(III)-D1	0.42	0.88			4.2 ± 0.8	
	Fe(II)-D2	1.27	2.55			1.6 ± 0.9	
W9	Fe(III)-S1	0.52		−0.10	42.7	55.4 ± 3.3	0.60
	Fe(III)-S2	0.42		0.09	44.9	41.1 ± 3.3	
	Fe(III)-D1	0.49	0.73			2.6 ± 0.5	
	Fe(II)-D2	1.12	2.58			0.9 ± 0.5	
W10	Fe(III)-S1	0.54		−0.11	42.4	51.8 ± 2.3	0.81
	Fe(III)-S2	0.42		0.11	44.9	43.2 ± 2.3	
	Fe(III)-D1	0.52	0.82			3.2 ± 0.6	
	Fe(II)-D2	1.24	2.96			1.7 ± 0.5	
W11	Fe(III)-S1	0.55		−0.10	42.5	51.3 ± 2.1	0.71
	Fe(III)-S2	0.42		0.07	45.1	45.4 ± 2.1	
	Fe(III)-D1	0.43	0.91			2.8 ± 0.3	
	Fe(II)-D2	1.20	2.90			0.5 ± 0.3	
W12	Fe(III)-S1	0.51		−0.14	40.8	54.4 ± 2.6	0.84
	Fe(III)-S2	0.45		0.10	44.5	45.6 ± 2.6	
W14	Fe(III)-S1	0.55		−0.08	42.3	56.9 ± 2.2	0.81
	Fe(III)-S2	0.40		0.07	45.1	39.8 ± 2.2	
	Fe(III)-D1	0.54	0.83			2.2 ± 0.4	
	Fe(II)-D2	1.12	2.70			1.0 ± 0.3	

[a]Center shift with respect to α-$^{57}Fe^0$. [b]Quadrupole splitting. [c]Quadrupole shift ($\epsilon = \Delta E_Q/2$). [d]Mean hyperfine field. [e]Spectral contribution and corresponding fit error. [f]Fit accuracy. [g]Species assignments: Fe(III)-S1: ferrihydrite, Fe(III)-S2: lepidocrocite, Fe(III)-D1: Fe(III)-OM complexes, Fe(II)-D2: adsorbed Fe(II).

previous reports on freshwater suspended particulate matter and flocs,[1,4,5] the flocs were significantly enriched in trace metal(loid)s (SI Table S1). Floc As concentrations varied between 34.2 and 2620 mg/kg; in some samples exceeding those of the underlying peat (≤1800 mg/kg).[11]

ATR-FTIR spectra of the flocs were similar, though they differed from spectra of humic acid, polysaccharide, and Fe(III)-(oxyhydr)oxide reference compounds (SI Figure S4). Detailed peak assignments are provided in the SI (Table S2). The dominating features in all spectra indicated C−O/C═O stretching (1052 and 1631/cm), O−H stretching (3284/cm), and C−H deformations (1375/cm). Despite sample complexity and band overlap, these results suggest that floc OM is primarily composed of EPS of microorganisms dominated by acid carbohydrates.

Synchrotron X-ray diffraction patterns of the flocs showed several diffuse scattering peaks with maxima corresponding to *d*-values of 4.0, 3.4, 2.5, 1.9, and 1.5 Å (SI Figure S5A). The broad 4.0-Å peak originates from diffuse scattering of OM, and the remaining features are consistent with nanometer-sized Fe(III)-(oxyhydr)oxides such as ferrihydrite. Additionally, the flocs comprised minor quantities of primary minerals such as quartz, phyllosilicates (biotite, muscovite, chlorite) and plagioclase (SI Figure S5B).

Iron Speciation: Mössbauer Spectroscopy. All samples displayed the superparamagnetic characteristics of poorly crystalline Fe minerals, as seen by the paramagnetic doublet recorded at 295 K and a magnetically ordered sextet at 5 K (Figure 1 and SI Figure S7). The 295-K spectra required a two site model corresponding to an Fe(III) and Fe(II) species (SI Figure S8). Fits obtained for the 295-K spectra are displayed in Figure 1A and SI Figure S7A, and their fit parameters are reported in SI Table S3. Populations calculated for the Fe(III) phase were ∼96%, with nearly identical CS values of ∼0.36 mm/s and mean quadrupole splittings (ΔE_Q) of 0.76−0.80 mm/s. These parameters are consistent with poorly crystalline Fe(III)-(oxyhydr)oxides such as ferrihydrite.[10] The contribu-

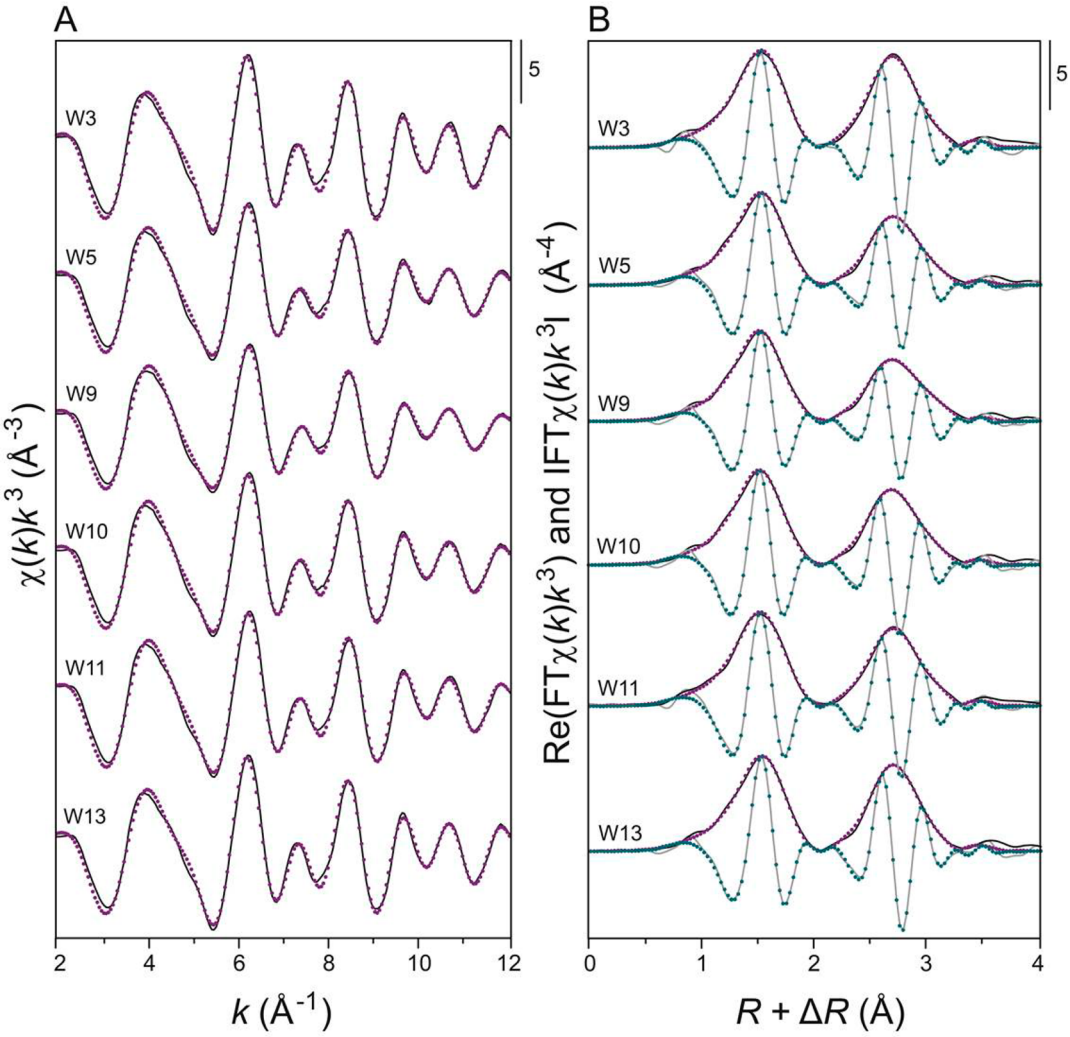

Figure 2. (A) Iron K-edge EXAFS spectra and (B) their Fourier-transform real parts and magnitudes of selected floc samples. Solid lines indicate experimental data and dotted lines show the model fits. Additional spectra are shown in SI Figure S10 and all EXAFS parameters are reported in Table 2

tion of the Fe(II) doublet to the total spectral area was estimated to be ~4% for all samples (SI Table S3).

Spectra collected at 5 K presented an asymmetry in the sextet feature, requiring the use of two sextets (denoted Fe(III)-S1 and Fe(III)-S2) in order to accurately fit the data (Figure 1B and SI Figure S7B, Table 1). While the 295-K spectra indicated the presence of ferrihydrite, analyses of the 5-K spectra found much lower hyperfine field values than would be expected. Two-line and 6-line ferrihydrite typically have hyperfine fields of 45−50 T,[10,23−25] whereas the observed hyperfine fields were 40.8−42.7 T (Fe(III)-S1) and 44.5−46.1 T (Fe(III)-S2) (Table 1). Eusterhues et al.[24] demonstrated that the hyperfine field of ferrihydrite is strongly influenced by OM content, and decreased from 49.5 to 46.0 T as the initial molar C/Fe ratio in their ferrihydrite syntheses was increased from 0 to 2.28. Considering that the 5-K quadrupole shifts (−0.08 to −0.14 mm/s) of the Fe(III)-S1 site match values reported for ferrihydrite,[10] the results imply that ferrihydrite constituted 51−59% of total floc-Fe (Table 1). A further analysis of Fe(III)-S1 subcomponents indicated a wide range in hyperfine fields (22.5−48.5 T), suggesting a broad particle-size distribution of ferrihydrite and/or variable structure perturbations due to sorption of diamagnetic elements such as C or Si[24,26] (SI Section 8 and SI Table S1).

For the Fe(III)-S2 site, quadrupole splittings of 0.07−0.13 mm/s and hyperfine fields of 44.5−46.1 T accord with lepidocrocite (γ-FeOOH).[25,27] Although this mineral comprised 34−46% of total floc-Fe (Table 1), it was not positively identified by SXRD (SI Figure S6), indicating a small coherent scattering domain (CSD) size similar to that of ferrihydrite (2−5 nm).

With the exception of sample W12, all 5-K spectra required two additional doublets corresponding to an Fe(III) and Fe(II) species (denoted Fe(III)-D1 and Fe(II)-D2). The 5-K Fe(III)-D1 doublet, with CS and ΔE_Q values of 0.42−0.54 and 0.73−0.97 mm/s, respectively, comprised 2.2−4.5% of total Fe and most likely originates from Fe(III)-OM complexes.[28] The 5-K CS (1.12−1.27 mm/s) and ΔE_Q values (2.55−2.96 mm/s) of the Fe(II)-D2 doublet (Table 1) agree with Fe(II) in a relatively undistorted octahedral oxygen environment.[29] Since no magnetic ordering was observed for the Fe(II) doublet at 5 K, it most likely originates from small amounts (0.5−2.7%) of adsorbed Fe(II)[30] (Table 1).

Iron Speciation: X-ray Absorption Spectroscopy. The speciation of Fe was additionally investigated by XAS.

Table 2. Shell-Fit Parameters Determined from Fe K-edge EXAFS Spectra of Floc Samples.[a]

			Fe−O1		Fe−O2		Fe−Fe1		Fe−Fe2		Fe−Fe3				
sample	As (mg/kg)	Fe (g/kg)	N[b]	R[c] (Å)	N	R (Å)	N	R (Å)	N	R (Å)	N	R (Å)	ΔE_0[d] (eV)	NSSR[e] (%)	red. χ^2[f]
W1	105	91.9	2.4(1)	1.94(1)	2.2(2)	2.06(1)	1.7(1)	3.06(1)	1.8(2)	3.43(1)	0.7(2)	3.61(2)	0.8(6)	0.6	100
W2	44.6	86.0	2.4(2)	1.93(1)	2.2(2)	2.05(1)	1.9(1)	3.06(1)	1.9(3)	3.44(1)	0.8(2)	3.63(2)	1.0(7)	0.6	84
W3	2620	199	2.3(2)	1.94(1)	2.3(3)	2.05(1)	2.7(1)	3.07(1)	1.6(3)	3.44(1)	0.8(2)	3.64(1)	0.8(7)	0.6	877
W4	50.4	110	2.4(2)	1.94(1)	2.2(2)	2.05(1)	1.9(1)	3.06(1)	1.7(3)	3.44(1)	0.7(2)	3.62(2)	0.7(7)	0.7	138
W5	1100	63.8	2.4(2)	1.94(1)	2.2(2)	2.06(1)	1.9(1)	3.07(1)	1.6(3)	3.44(1)	0.7(2)	3.63(2)	0.9(7)	0.6	112
W8	103	93.7	2.4(2)	1.94(1)	2.2(3)	2.06(1)	2.0(1)	3.06(1)	1.8(3)	3.43(1)	0.8(2)	3.63(2)	0.4(6)	0.6	102
W9	1280	134	2.2(2)	1.93(1)	2.4(2)	2.04(1)	2.0(1)	3.06(1)	1.8(3)	3.44(1)	0.7(2)	3.63(2)	0.1(7)	0.6	318
W10	1330	99.4	2.4(2)	1.94(1)	2.2(2)	2.06(1)	2.1(1)	3.06(1)	1.9(3)	3.44(1)	0.8(2)	3.63(1)	1.0(7)	0.6	103
W11	525	128	2.3(2)	1.93(1)	2.3(2)	2.05(1)	2.2(1)	3.07(1)	1.8(3)	3.44(1)	0.8(2)	3.63(2)	0.8(6)	0.6	720
W12	134	192	2.4(3)	1.94(1)	2.3(3)	2.05(1)	2.7(1)	3.07(1)	1.7(4)	3.43(1)	0.9(3)	3.63(2)	0.6(8)	0.7	228
W13	1230	221	2.3(3)	1.94(1)	2.2(3)	2.05(1)	2.5(1)	3.07(1)	1.6(2)	3.44(1)	0.8(2)	3.64(2)	0.8(7)	0.7	217

[a]The amplitude reduction factor, S_0^2, was set to 0.9. Parameter uncertainties are presented for the last significant figure. The Debye−Waller parameters, σ^2, were fixed to 0.004 Å^2 (Fe−O1/2), 0.006 Å^2 (Fe−Fe1/3), and 0.008 Å^2 (Fe−Fe2). [b]Path degeneracy (coordination number). [c]Mean half path length. [d]Energy-shift parameter. [e]Normalized sum of squared residuals $(100\sum_i(\text{data}_i\text{-fit}_i)^2/\sum_i\text{data}^2)$. [f]Fit accuracy; reduced $\chi^2 = (N_{idp}/N_{pts})\sum_i((\text{data}_i\text{-fit}_i)/\varepsilon_i)^2(N_{idp}\text{-}N_{var})^{-1}$. N_{idp}, N_{pts} and N_{var} are, respectively, the number of independent points in the model fit (29.3), the total number of data points (241), and the number of fit variables (11). ε_i is the uncertainty of the ith data point. Note: Models also included a triangular Fe−O−O multiple scattering path defined as follows: $N = 4\sum N_{Fe-O}$, $R = [(N_{Fe-O1}R_{Fe-O1})/\sum N_{Fe-O}+(N_{Fe-O2}R_{Fe-O2})/\sum N_{Fe-O}](1+\sqrt{2}/2)$, and $\sigma^2 = 2\sigma^2_{Fe-O}$. This path improved the reduced χ^2 by 38% on average.

Consistent with the predominance of Fe(III) in the flocs (Table 1), all XANES spectra (n = 11) showed first-derivative maxima at ∼7128 eV, consistent with Fe(III) reference compounds (SI Figure S9A). Because of the low proportions of Fe(III)-OM complexes and Fe(II) in the samples (Table 1), only ferrihydrite and lepidocrocite were required as reference compounds in linear combination fit (LCF) analyses to adequately fit the samples' EXAFS spectra (SI Figure S9B). Accordingly, the flocs contained 50−70% ($\bar{x}$ = 63) ferrihydrite, the rest being lepidocrocite (SI Table S5). After correcting for the minor Fe species detected by Mössbauer spectroscopy, the LCF results were in reasonable agreement with the Mössbauer data (SI Table S6).

Shell-fit analyses of k^3-weighted Fe K-edge EXAFS spectra were performed in order to explore the local coordination environment of Fe in selected floc samples. A preliminary multidata set (n = 11) R-space fit of the first Fourier-transform peak conducted over $R + \Delta R$ = 0.9−2.2 Å revealed that two Fe−O paths were required to accurately model the first O shell. This fit delivered average Fe−O distances of 1.94 ± 0.01 and 2.05 ± 0.01 Å and two similar Debye−Waller parameters, σ^2, of 0.004 ± 0.001 Å^2. In subsequent fits extended to 4.5 Å ($R + \Delta R$), the Debye−Waller parameters of the Fe−O paths were fixed to this value. The final fit model contained three additional Fe−Fe paths representative of edge- (Fe−Fe1), double corner- (Fe−Fe2), and single corner-sharing Fe (Fe−Fe3). F-tests concluded that the inclusion of the latter path significantly improved the fits (SI Table S7). The Debye−Waller parameters of the Fe paths were initially fit at 0.006 Å^2 (Fe−Fe1/3) and 0.008 Å^2 (Fe−Fe2), and later fixed to reduce parameter correlations. These values are consistent with a mixture of ferrihydrite and lepidocrocite.[31−33] The final model fits are illustrated in Figure 2 and SI Figure S10 and the corresponding EXAFS parameters are summarized in Table 2. For all floc samples, the first shell was fit on average with 2.3 O atoms at 1.94 Å and 2.3 O atoms at 2.05 Å. The weighted average Fe−O distance was 1.99 Å, in accordance with octahedrally coordinated ^{VI}Fe(III) in Fe(III)-(oxyhydr)-oxides,[31−33] whereas the degeneracy (N) sum of the Fe−O paths was much lower than expected for ^{VI}Fe(III). This result suggests significant octahedral distortion caused by broad Fe−O distance distributions leading to destructive interference of individual Fe−O scattering waves.[32,34] Maillot et al.[35] attributed a similar underestimation of $\sum N_{Fe-O}$ in 2-line and 6-line ferrihydrite to tetrahedrally coordinated ^{IV}Fe(III). Assuming a Gaussian distribution of Fe−O1 distances ($\bar{x}$ = 1.94 Å, σ = 0.063 Å), ∼26% of the O1 atoms in the flocs would have Fe−O distances <1.9 Å qualifying for ^{IV}Fe(III).[31,36] Iron shells fit at 3.06 ± 0.01 and 3.44 ± 0.01 Å are characteristic of edge- and double corner-sharing FeO_6 octahedra in FeOOH polymorphs.[37] The typical EXAFS-derived number of Fe1 and Fe2 atoms in ferrihydrite is 1.3−4.0 ($\bar{x}$ = 2.4) and 1.4−2.6 ($\bar{x}$ = 1.9), respectively.[31−34,38] In contrast, six Fe1 atoms are expected from the crystal structure of lepidocrocite, which does not possess double corner-sharing FeO_6 octahedra.[39] Considering the abundance of both minerals in the flocs determined by LCF (SI Table S5), one would expect an average N_{Fe-Fe1} and N_{Fe-Fe2} of 3.8 and 1.2, respectively. While the average fit N_{Fe-Fe2} of 1.7 ± 0.3 is close to the expected value, an N_{Fe-Fe1} of only 2.1 ± 0.4 is significantly lower than anticipated (Table 2). For all floc samples, 0.8 ± 0.1 Fe atoms were additionally fit at 3.63 ± 0.01 Å (Table 2). This Fe−Fe distance complies with the 3.66 Å inferred from EXAFS spectroscopy for single corner-sharing FeO_6 octahedra in lepidocrocite.[37] As the nominal N for single corner-sharing FeO_6 octahedra in lepidocrocite is two,[37,39] the degeneracy of the Fe−Fe3 path agrees well with the <50% fractions of lepidocrocite in the samples (Table 2 and SI Table S5). Combined, these results suggest that lepidocrocite in the flocs is highly disordered. Because the Fe−Fe3 path parameters were close to theoretical (N) or experimental (R) values reported for lepidocrocite, the low N_{Fe-Fe1}/N_{Fe-Fe3} ratios of floc lepidocrocite inferred from the EXAFS data may originate from a significant shortening of the dioctahedral chains in the lepidocrocite structure. It is worth noting that the inclusion of an Fe−C path (R = 2.8−2.9 Å)[16,17,40] led to negative N_{Fe-C} in all cases, implying that Fe(III)-OM complexes are sparse (Table 1) and that chemisorbed organic ligands do not cover the entire surface of the nanocrystalline Fe(III) minerals observed in the flocs.

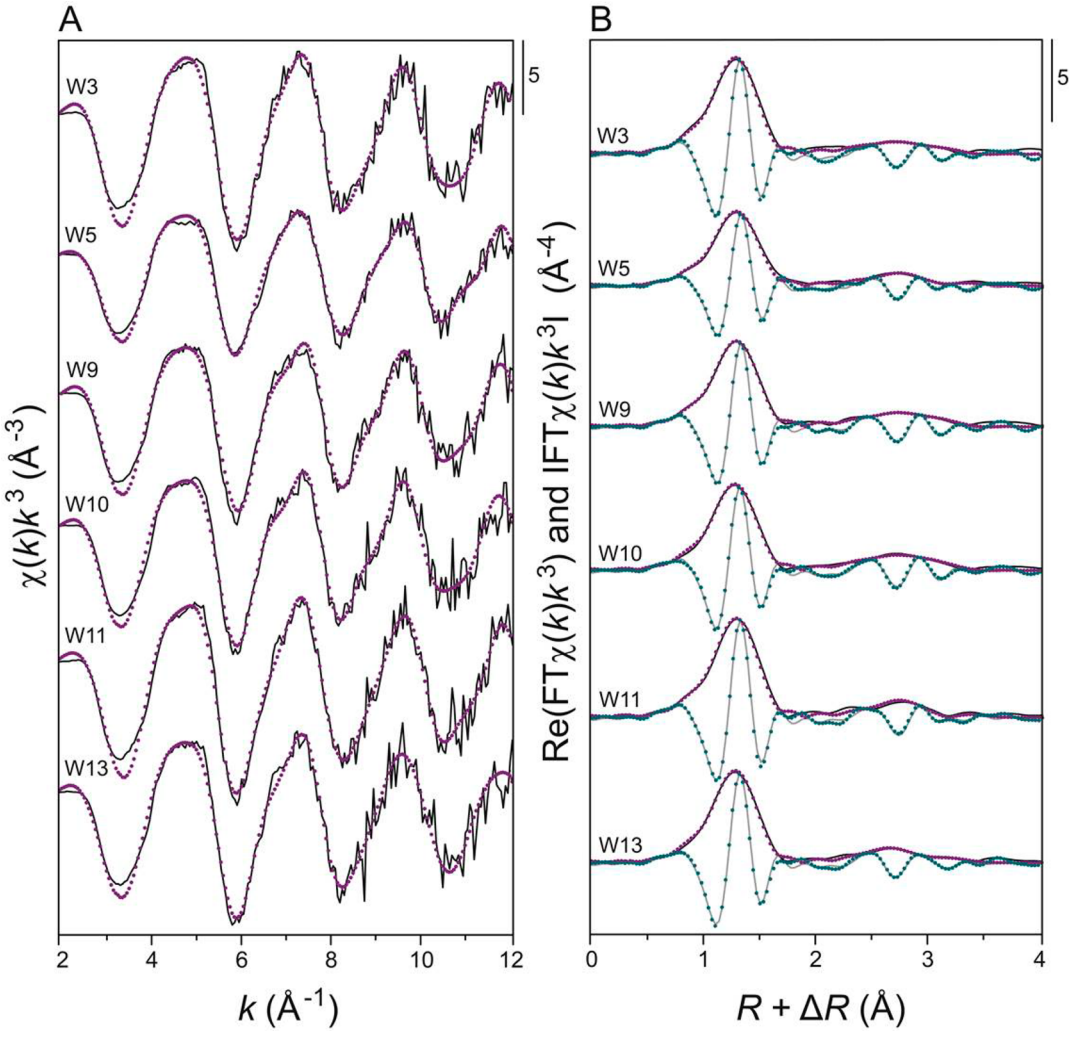

Figure 3. (A) Arsenic K-edge EXAFS spectra and (B) their Fourier-transform real parts and magnitudes of floc samples. Solid lines indicate experimental data and dotted lines show the model fits. The corresponding EXAFS parameters are reported in Table 3

Table 3. Shell-fit parameters determined from As K-edge EXAFS spectra of floc samples.[a]

			As–O			As–O–O[f]	As–Fe[g]				
sample	As (mg/kg)	As(V)[b] (%)	N[c]	R[d] (Å)	σ^2[e] (Å^2)	R (Å)	N	R (Å)	ΔE_0[h] (eV)	NSSR[i] (%)	red. χ^2[j]
W3	2620	80	4.2(3)	1.70(1)	0.003(1)	3.12(6)	2.1(6)	3.33(2)	6.4(12)	1.3	6.3
W5	1100	71	3.2(3)	1.71(1)	0.003(1)	3.13(5)	1.5(5)	3.31(2)	5.9(14)	1.7	16
W9	1280	72	3.9(3)	1.71(1)	0.003(1)	3.13(5)	2.6(6)	3.32(2)	5.7(14)	1.6	13
W10	1330	71	4.0(3)	1.70(1)	0.003(1)	3.13(6)	2.8(5)	3.32(1)	4.9(12)	1.2	4.9
W11	525	84	4.1(4)	1.70(1)	0.003(1)	3.10(5)	2.1(6)	3.34(2)	6.6(14)	1.6	11
W13	1230	75	4.2(4)	1.70(1)	0.003(1)	3.10(6)	2.1(6)	3.32(2)	5.2(14)	1.5	6.6

[a]The amplitude reduction factor, S_0^2, was set to 1.0. Parameter uncertainties are presented for the last significant figure. [b]Fraction (f) of As(V) determined by linear combination fitting (SI Figure S11). [c]Path degeneracy (coordination number). [d]Mean half path length. [e]Debye–Waller parameter. [f]Triangular multiple scattering path defined as follows: $N = 12f_{As(V)}+6f_{As(III)}$ and $\sigma^2 = 2\sigma^2_{As-O}$. [g]Debye–Waller parameter fixed to 0.010 Å^2. [h]Energy-shift parameter. [i]Normalized sum of squared residuals $(100\sum_i(data_i\text{-}fit_i)^2/\sum_i data^2)$. [j]Fit accuracy; reduced $\chi^2 = (N_{idp}/N_{pts})\sum_i((data_i\text{-}fit_i)/\varepsilon_i)^2(N_{idp}\text{-}N_{var})^{-1}$. N_{idp}, N_{pts} and N_{var} are, respectively, the number of independent points in the model fit (18.1), the total number of data points (201), and the number of fit variables (7). ε_i is the uncertainty of the i^{th} data point.

Arsenic Speciation: X-ray Absorption Spectroscopy. The speciation of As in the flocs was determined using bulk XAS. Analyzed floc samples (n = 6) exhibited two maxima in their first XANES derivatives located at ∼11869 and ∼11873 eV (SI Figure S11A), indicating the presence of both As(III) and As(V). Initial EXAFS LCFs including arsenobetaine and dimethylarsinic acid as fit references delivered negative fit fractions for these methylated As(V) compounds. Consequently, LCF analyses were conducted with only two inorganic reference compounds: arsenite- and arsenate-adsorbed ferrihydrite (SI Figure S11B). The resulting fits revealed that the flocs primarily contained Fe-associated arsenate, comprising 71–84% ($\bar{x}$ = 75) of the total As (SI Table S8).

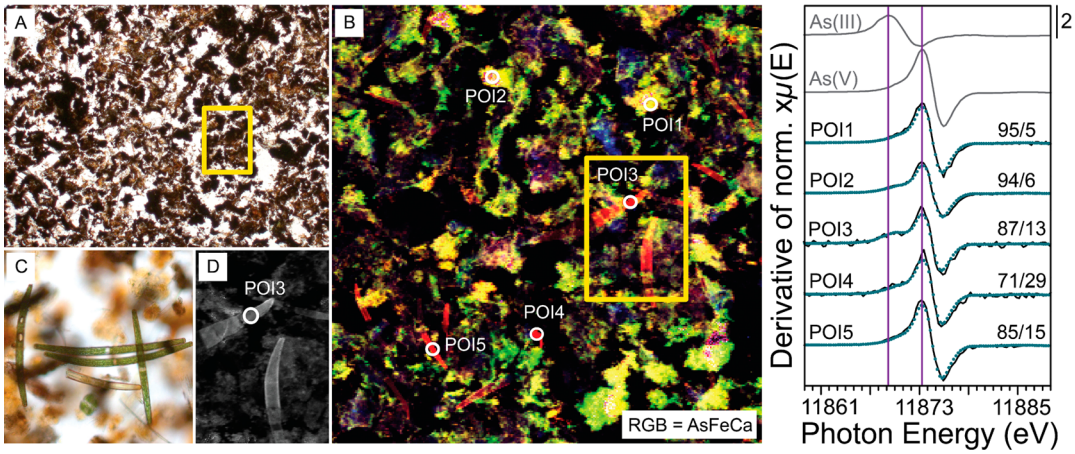

Figure 4. (A, C) Light microscopy and (B, D) μ-XRF maps collected at 13 keV for floc sample W3. Image sizes are (H × V) (A) 4 × 3 mm^2, (B) 1.5 × 1.5 mm^2, (C) 0.5 × 0.5 mm^2, and (D) 0.3 × 0.5 mm^2. Map (B) shows the distributions of As, Fe, and Ca, whereas the gray scale map (D) shows solely the distribution of As (white corresponds to high As concentrations). The yellow insets in (A) and (B) correlate with map (D). The right panel shows the first derivatives of As K-edge XANES spectra collected at selected points of interest (POIs) indicated in map (B). Their corresponding LCFs using arsenite/arsenate-adsorbed ferrihydrite as fit references are shown as dotted lines (fit range: −20 to 30 eV (E-E_0), initial fit sums: 100 ± 10%, normalized sum of squared residuals: 0.09−0.54%). The LCF results are reported as As(V)/As(III) ratios. Additional μ-XRF maps are shown in SI Figures S12 and S13.

In order to explore the local coordination environment of As in the flocs, shell-fits of k^3-weighted EXAFS spectra were performed in R-space over 0.9−3.8 Å. All Fourier-transformed spectra showed a pronounced peak at ∼1.3 Å, which arises from first-shell O atoms, and a small broad peak at ∼2.2−3.5 Å, most likely originating from multiple scattering in AsO_3 and AsO_4 polyhedra and distant Fe shells (Figure 3B).[11,14,16] Initial fits with an As−S path (R = 2.2−3.1 Å)[11,14,41] or an As−C path (R = 2.7−3.2 Å)[14,16] proved unsuccessful, implying that floc As(III) is not coordinated to reduced S species as evidenced in the *Gola di Lago* peat[11,13,15] or bound to hydroxylic/phenolic groups of floc OM. Attempts to fit As−Ca or As−Al paths[42,43] to the data also failed, suggesting As sorption to Ca/Al-OM complexes and Al minerals was also negligible. Therefore, final shell-fit models contained only As−O, As−O−O, and As−Fe scattering paths. The Debye−Waller parameters of the As−Fe path were first fit and later fixed to an average value of 0.010 Å^2; close to the average Debye−Waller parameter (0.009 Å^2) determined for arsenite/arsenate-adsorbed Fe(III)-(oxyhydr)-oxides.[33,41,44] The resulting fits are shown in Figure 3 and their EXAFS parameters are reported in Table 3.

Between 3.2 and 4.2 O atoms were fit at an average distance of 1.70 ± 0.01 Å. This distance is reasonably expected for a mixture of arsenite and arsenate dominated by the latter.[33,41] Additionally, the fits delivered 1.5−2.8 Fe atoms at a distance of 3.31−3.34 Å (Table 3). These distances are similar to values reported for arsenite/arsenate sorbed to Fe(III)-(oxyhydr)-oxides[33,41] and Fe(III)-OM complexes,[16,17] and signify the formation of monodentate-binuclear ("bridging") As complexes in the flocs. Because no Fe shell could be fit at ∼2.9 Å, it follows that bidentate-mononuclear arsenite surface complexes[41,44] are negligible in the flocs, in agreement with an average N_{As-Fe} of 2.2 ± 0.6 (Table 3).

In summary, As shell-fit analyses document that despite abundant OM, the floc-As was entirely bound to Fe(III)-(oxyhydr)oxides in a monodentate−binuclear fashion. The absence of ternary As-Fe(III)-OM complexes in the flocs accords with the low content of Fe(III)-OM complexes (Table 1), and the impossibility of fitting an As−C path with R = 2.7−3.2 Å implies that arsenite has a low affinity toward the carbohydrate-dominated OM (SI Figure S4). This result in turn suggests that phenolic OH groups were mainly responsible for the direct binding of arsenite to peat OM under anoxic conditions observed by Hoffmann et al.[16]

Arsenic Distribution and Local Speciation. Selected floc samples were additionally analyzed by μ-XRF spectrometry and μ-XANES spectroscopy. Figure 4A illustrates a light microscopy image of sample W3, and Figure 4B the corresponding μ-XRF map showing the distributions of As, Fe, and Ca. Additional μ-XRF maps and XRF spectra of this sample can be found in SI Figures S12 and S13. The results show that As in the flocs was primarily associated with Fe, which was also correlated with other trace elements such as Zn and Ni (SI Figure S12). Despite the appearance of As−S correlations in the flocs (SI Figure S12), no S coordination of As was observed (Table 3). This finding suggests that reduced organic S moieties in floc OM are far less abundant compared to reactive ≡FeOH sites of Fe(III)-(oxyhydr)oxides.[45] Intense As hotspots in the elemental maps were associated with *Closterium* spp. (Figure 4B−D), a freshwater green algae common in peatlands.[46,47] Green algae are known to effectively take-up trace metal(loid)s,[48,49] and bioaccumulation of As in green algae has been shown to be accompanied by As(V) reduction and methylation reactions.[50−52] Consistent with these findings, μ-XANES spectra collected at algae-specific POIs (3−5) revealed that As(V) comprised 71−87% of the total As, whereas the As(V) fraction at Fe-rich POIs (1, 2) was significantly higher (Figure 4).

Environmental Implications. This study shows that Fe-rich flocs in surface waters of the minerotrophic *Gola di Lago* peatland contain primarily ferrihydrite and "X-ray amorphous" lepidocrocite. The lepidocrocite is characterized by a CSD size not significantly exceeding that of ferrihydrite (2−5 nm). Both minerals form by the rapid oxidation of Fe(II), diffusing from the uppermost peat layers, in an organic matrix of microbial EPS dominated by acid carbohydrates. Elevated solution concentrations of arsenate, phosphate, Si, and humic substances have been shown to impair the formation of lepidocrocite in

favor of ferrihydrite.[32,53,54] Based on solution data (SI Table S1), it is plausible that both Si and floc EPS impeded the formation of lepidocrocite and effectively inhibited its crystal growth. Due to their low CSD size, floc Fe(III)-(oxyhydr)-oxides are efficient sorbents for As and other trace metal(loid)s (SI Figure S12).[1,4,5] Since Fe was abundant in the flocs and the content of Fe(III)-OM complexes low, ternary As complexes[16−18] and sulfhydryl-coordinated As[11,13,14,45] were not of quantitative importance.

Recently, Riedel et al.[55] reported that precipitation of Fe with DOC (62−258 mg/L) in oxygenated fen pore waters removed primarily plant-derived aromatic and pyrogenic C, whereas carboxyl-rich aliphatic acids remained in solution. The selective incorporation of aromatic and pyrogenic C in their Fe precipitates is contrary to our observation and those of others[1−3,5] showing that floc Fe(III)-(oxyhydr)oxides are mainly associated with carbohydrate-rich EPS. This discrepancy most likely results from an abundance of EPS in the *Gola di Lago* surface streams, either suspended or associated with plants and their debris, which form organic interfaces for Fe(II) oxidation and Fe(III) mineral precipitation. Thus, the major pathway of floc formation differs from the "classical" coprecipitation process by which OM is selectively removed from solution via Fe(III)-(oxyhydr)oxide precipitation.[24,28,38]

The presence of nanometer-sized Fe(III) minerals embedded in an organic matrix of EPS has several potential implications for the cycling of trace elements in wetlands. A combination of nanocrystallinity and limited particle aggregation[1,3,6] renders floc Fe(III)-(oxyhydr)oxides prone to photoreduction[56] as well as ligand-promoted dissolution reactions,[57] causing the release of associated trace metal(loid)s into solution. Owing to their high density and thus gravitational settling under low-flow conditions (SI Figure S1), flocs are likely to become buried and thus subject to Fe- and SO_4-reducing conditions over time. Biotically formed Fe(II) and bisulfide are effective reductants for Fe(III)-(oxyhydr)oxides, and trigger the formation of polysulfides, mackinawite (FeS), and/or pyrite (FeS_2).[58−60] The low crystallinity of floc Fe(III)-(oxyhydr)oxides may facilitate these (mineral) transformations. Arsenic released from buried flocs may then become immobilized by Fe sulfide minerals,[41] mixed-valence Fe minerals,[20,61] or precipitate as Fe sulfoarsenide or As sulfide;[13,62] a scenario explaining the occurrence of realgar (α-As_4S_4) and arsenopyrite (FeAsS) in shallow peat layers of the *Gola di Lago* peatland.[11,13] Collectively, our results imply that freshwater flocs play a vital role in the speciation and cycling of trace metal(loid)s in wetlands and that their reductive transformation warrants further research.

■ ASSOCIATED CONTENT

Supporting Information

Sampling locations, details on XAS data collection and reduction, concentration analyses, microscopy images, ATR-FTIR spectra, SXRD patterns, additional Mössbauer spectra, and additional XAS results and μ-XRF maps. This material is available free of charge via the Internet at http://pubs.acs.org/.

■ AUTHOR INFORMATION

Corresponding Author

*Phone: +41-44-6336024; fax: +41-44-6331118; e-mail: christian.mikutta@env.ethz.ch.

Notes

The authors declare no competing financial interest.

■ ACKNOWLEDGMENTS

We are grateful to S. Hug (Eawag) for assisting us in collecting ATR-FTIR spectra and to J. Brahney (University of British Columbia) for helpful discussions. We acknowledge ELETTRA, ESRF, SLS, and APS (a U.S. Department of Energy Office of Science User Facility operated by Argonne National Laboratory, contract No. DE-AC02-06CH11357) for the provision of synchrotron radiation facilities and thank G. Aquilanti (ELETTRA, XAFS beamline), G. Agostini (ESRF, beamline BM23), A. Cervellino (SLS, beamline X04SA), and A. Lanzirotti and M. Newville (APS, beamline 13-ID-E) for their support during the synchrotron measurements. This project was funded by the SNSF (Project 200021_127157).

■ REFERENCES

(1) Plach, J. M.; Elliott, A. V. C.; Droppo, I. G.; Warren, L. A. Physical and ecological controls on freshwater floc trace metal dynamics. *Environ. Sci. Technol.* **2011**, *45*, 2157−2164.
(2) Droppo, I. G. Rethinking what constitutes suspended sediment. *Hydrol. Process.* **2001**, *15*, 1551−1564.
(3) Droppo, I. G.; Leppard, G. G.; Flannigan, D. T.; Liss, S. N. The freshwater floc: A functional relationship of water and organic and inorganic floc constituents affecting suspended sediment properties. *Water, Air, Soil Pollut.* **1997**, *99*, 43−53.
(4) Elliott, A. V. C.; Plach, J. M.; Droppo, I. G.; Warren, L. A. Comparative floc-bed sediment trace element partitioning across variably contaminated aquatic ecosystems. *Environ. Sci. Technol.* **2012**, *46*, 209−216.
(5) Plach, J. M.; Warren, L. A. Differentiating natural organic matter roles in freshwater floc and bed sediment lead dynamics. *Chem. Geol.* **2012**, *304*, 97−105.
(6) Larsen, L. G.; Harvey, J. W.; Crimaldi, J. P., Morphologic and transport properties of natural organic floc. *Water Resour. Res.* **2009**, *45*.
(7) Larsen, L. G.; Harvey, J. W.; Noe, G. B.; Crimaldi, J. P., Predicting organic floc transport dynamics in shallow aquatic ecosystems: Insights from the field, the laboratory, and numerical modeling. *Water Resour. Res.* **2009**, *45*.
(8) Elliott, A. V. C.; Warren, L. A. Microbial engineering of floc Fe and trace metal geochemistry in a circumneutral, remote lake. *Environ. Sci. Technol.* **2014**, *48*, 6578−6587.
(9) Sundman, A.; Karlsson, T.; Persson, P. An experimental protocol for structural characterization of Fe in dilute natural waters. *Environ. Sci. Technol.* **2013**, *47*, 8557−8564.
(10) Murad, E. The Mössbauer spectrum of 'well'-crystallized ferrihydrite. *J. Magn. Magn. Mater.* **1988**, *74*, 153−157.
(11) Langner, P.; Mikutta, C.; Kretzschmar, R. Arsenic sequestration by organic sulphur in peat. *Nature Geosci.* **2012**, *5*, 66−73.
(12) Zayre, I.; González, A; Krachler, M.; Cheburkin, A. K.; Shotyk, W. Spatial distribution of natural enrichments of arsenic, selenium, and uranium in a minerotrophic peatland, Gola di Lago, Canton Ticino, Switzerland. *Environ. Sci. Technol.* **2006**, *40*, 6568−6574.
(13) Langner, P.; Mikutta, C.; Suess, E.; Marcus, M. A.; Kretzschmar, R. Spatial distribution and speciation of arsenic in peat studied with microfocused X-ray fluorescence spectrometry and X-ray absorption spectroscopy. *Environ. Sci. Technol.* **2013**, *47*, 9706−9714.
(14) Hoffmann, M.; Mikutta, C.; Kretzschmar, R. Bisulfide reaction with natural organic matter enhances arsenite sorption: Insights from X-ray absorption spectroscopy. *Environ. Sci. Technol.* **2012**, *46*, 11788−11797.
(15) Langner, P.; Mikutta, C.; Kretzschmar, R. Oxidation of organosulfur-coordinated arsenic and realgar in peat: Implications for the fate of arsenic. *Environ. Sci. Technol.* **2014**, *48*, 2281−2289.

(16) Hoffmann, M.; Mikutta, C.; Kretzschmar, R. Arsenite binding to natural organic matter: Spectroscopic evidence for ligand exchange and ternary complex formation. *Environ. Sci. Technol.* **2013**, *47*, 12165−12173.
(17) Mikutta, C.; Kretzschmar, R. Spectroscopic evidence for ternary complex formation between arsenate and ferric iron complexes of humic substances. *Environ. Sci. Technol.* **2011**, *45*, 9550−9557.
(18) Mikutta, C.; Frommer, J.; Voegelin, A.; Kaegi, R.; Kretzschmar, R. Effect of citrate on the local Fe coordination in ferrihydrite, arsenate binding, and ternary arsenate complex formation. *Geochim. Cosmochim. Acta* **2010**, *74*, 5574−5592.
(19) Hohmann, C.; Winkler, E.; Morin, G.; Kappler, A. Anaerobic Fe(II)-oxidizing bacteria show As resistance and immobilize As during Fe(III) mineral precipitation. *Environ. Sci. Technol.* **2010**, *44*, 94−101.
(20) Wang, Y.; Morin, G.; Ona-Nguema, G.; Juillot, F.; Guyot, F.; et al. Evidence for different surface speciation of arsenite and arsenate on green rust: An EXAFS and XANES study. *Environ. Sci. Technol.* **2010**, *44*, 109−115.
(21) Smedley, P. L.; Kinniburgh, D. G. A review of the source, behaviour and distribution of arsenic in natural waters. *Appl. Geochem.* **2002**, *17*, 517−568.
(22) Willmott, P. R.; Meister, D.; Leake, S. J.; Lange, M.; Bergamaschi, A.; et al. The Materials Science beamline upgrade at the Swiss Light Source. *J. Synchrotron. Radiat.* **2013**, *20*, 667−682.
(23) Mikutta, C.; Mikutta, R.; Bonneville, S.; Wagner, F.; Voegelin, A.; et al. Synthetic coprecipitates of exopolysaccharides and ferrihydrite. Part 1: Characterization. *Geochim. Cosmochim. Acta* **2008**, *72*, 3292−3292.
(24) Eusterhues, K.; Wagner, F. E.; Häusler, W.; Hanzlik, M.; Knicker, H.; et al. Characterization of ferrihydrite-soil organic matter coprecipitates by X-ray diffraction and Mössbauer spectroscopy. *Environ. Sci. Technol.* **2008**, *42*, 7891−7897.
(25) Cornell, R. M.; Schwertmann, U. *The Iron Oxides: Structure, Properties, Reactions, Occurances and Uses*; Wiley-VCH: Weinheim, Germany, 2004.
(26) Schwertmann, U.; Friedl, J. I.; Kyek, A. Formation and properties of a continuous crystallinity series of synthetic ferrihydrites (2- to 6-line) and their relation to FeOOH forms. *Clay. Clay Miner.* **2004**, *52*, 221−226.
(27) Murad, E.; Schwertmann, U. The influence of crystallinity on the Mössbauer spectrum of lepidocrocite. *Mineral. Mag.* **1984**, *48*, 507−511.
(28) Schwertmann, U.; Wagner, F.; Knicker, H. Ferrihydrite-humic associations: Magnetic hyperfine interactions. *Soil Sci. Soc. Am. J.* **2005**, *69*, 1009−1015.
(29) Dyar, M. D.; Agresti, D. G.; Schaefer, M. W.; Grant, C. A.; Sklute, E. C. Mössbauer spectroscopy of earth and planetary materials. *Annu. Rev. Earth Pl. Sc.* **2006**, *34*, 83−125.
(30) Williams, A. G. B.; Scherer, M. M. Spectroscopic evidence for Fe(II)-Fe(III) electron transfer at the iron oxide-water interface. *Environ. Sci. Technol.* **2004**, *38*, 4782−4790.
(31) Manceau, A. Critical evaluation of the revised akdalaite model for ferrihydrite. *Am. Mineral.* **2011**, *96*, 521−533.
(32) Voegelin, A.; Kaegi, R.; Frommer, J.; Vantelon, D.; Hug, S. J. Effect of phosphate, silicate, and Ca on Fe(III)-precipitates formed in aerated Fe(II)- and As(III)-containing water studied by X-ray absorption spectroscopy. *Geochim. Cosmochim. Acta* **2010**, *74*, 164−186.
(33) Waychunas, G. A.; Rea, B. A.; Fuller, C. C.; Davis, J. A. Surface chemistry of ferrihydrite: Part 1. EXAFS studies of the geometry of coprecipitated and adsorbed arsenate. *Geochim. Cosmochim. Acta* **1993**, *57*, 2251−2269.
(34) Miot, J.; Benzerara, K.; Morin, G.; Kappler, A.; Bernard, S.; et al. Iron biomineralization by anaerobic neutrophilic iron-oxidizing bacteria. *Geochim. Cosmochim. Acta* **2009**, *73*, 696−711.
(35) Maillot, F.; Morin, G.; Wang, Y.; Bonnin, D.; Ildefonse, P.; et al. New insight into the structure of nanocrystalline ferrihydrite: EXAFS evidence for tetrahedrally coordinated iron(III). *Geochim. Cosmochim. Acta* **2011**, *75*, 2708−2720.
(36) Shmakov, A. N.; Kryukova, G. N.; Tsybulya, S. V.; Chuvilin, A. L.; Solovyeva, L. P. Vacancy ordering in γ-Fe_2O_3: Synchrotron X-ray powder diffration and high-resoultion electron microscopy studies. *J. Appl. Crystallogr.* **1995**, *28*, 141−145.
(37) Manceau, A.; Combes, J. M. Structure of Mn and Fe oxides and oxyhydroxides: A topological approach by EXAFS. *Phys. Chem. Miner.* **1988**, *15*, 283−295.
(38) Mikutta, C. X-ray absorption spectroscopy study on the effect of hydroxybenzoic acids on the formation and structure of ferrihydrite. *Geochim. Cosmochim. Acta* **2011**, *75*, 5122−5139.
(39) Zhukhlistov, A. P. Crystal structure of lepidocrocite FeO(OH) from the electron-diffractometry data. *Crystallogr. Rep.* **2001**, *46*, 730−733.
(40) Karlsson, T.; Persson, P. Coordination chemistry and hydrolysis of Fe(III) in a peat humic acid studied by X-ray absorption spectroscopy. *Geochim. Cosmochim. Acta* **2010**, *74*, 30−40.
(41) Farquhar, M. L.; Charnock, J. M.; Livens, F. R.; Vaughan, D. J. Mechanisms of arsenic uptake from aqueous solution by interaction with goethite, lepidocrocite, mackinawite, and pyrite: An X-ray absorption spectroscopy study. *Environ. Sci. Technol.* **2002**, *36*, 1757−1762.
(42) Bardelli, F.; Benvenuti, M.; Costagliola, P.; Di Benedetto, F.; Lattanzi, P.; et al. Arsenic uptake by natural calcite: An XAS study. *Geochim. Cosmochim. Acta* **2011**, *75*, 3011−3023.
(43) Arai, Y.; Elzinga, E. J.; Sparks, D. L. X-ray absorption spectroscopic investigation of arsenite and arsenate adsorption at the aluminum oxide-water interface. *J. Colloid Interface Sci.* **2001**, *235*, 80−88.
(44) Ona-Nguema, G.; Morin, G.; Juillot, F.; Calas, G.; Brown, G. E. EXAFS analysis of arsenite adsorption onto two-line ferrihydrite, hematite, goethite, and lepidocrocite. *Environ. Sci. Technol.* **2005**, *39*, 9147−9155.
(45) Hoffmann, M.; Mikutta, C.; Kretzschmar, R. Arsenite binding to sulfhydryl groups in the absence and presence of ferrihydrite: A model study. *Environ. Sci. Technol.* **2014**, *48*, 3822−3831.
(46) Neustupa, J.; Černá, K.; Šťastný, J. Diversity and morphological disparity of desmid assemblages in Central European peatlands. *Hydrobiologia* **2009**, *630*, 243−256.
(47) Coesel, P. F. M. Structural characteristics and adaptations of desmid communities. *J. Ecol.* **1982**, *70*, 163−177.
(48) Mahan, C. A.; Majidi, V.; Holcombe, J. A. Evaluation of the metal uptake of several algae strains in a multicomponent matrix utilizing inductively coupled plasma emission spectrometry. *Anal. Chem.* **1989**, *61*, 624−627.
(49) Maeda, S.; Nakashima, S.; Takeshita, T.; Higashi, S. Bioaccumulation of arsenic by freshwater algae and the application to the removal of inorganic arsenic from an aqueous phase. Part 2. By *Chlorella-Vulgaris* isolated from arsenic-polluted environment. *Sep. Sci. Technol.* **1985**, *20*, 153−161.
(50) Levy, J. L.; Stauber, J. L.; Adams, M. S.; Maher, W. A.; Kirby, J. K.; et al. Toxicity, biotransformation, and mode of action of arsenic in two freshwater microalgae (*Chlorella* sp and *Monoraphidium arcuatum*). *Environ. Toxicol. Chem.* **2005**, *24*, 2630−2639.
(51) Hasegawa, H.; Sohrin, Y.; Seki, K.; Sato, M.; Norisuye, K.; et al. Biosynthesis and release of methylarsenic compounds during the growth of freshwater algae. *Chemosphere* **2001**, *43*, 265−272.
(52) Knauer, K.; Hemond, H. Accumulation and reduction of arsenate by the freshwater green alga *Chlorella* sp (Chlorophyta). *J. Phycol.* **2000**, *36*, 506−509.
(53) Pédrot, M.; Le Boudec, A.; Davranche, M.; Dia, A.; Henin, O. How does organic matter constrain the nature, size and availability of Fe nanoparticles for biological reduction? *J. Colloid Interface Sci.* **2011**, *359*, 75−85.
(54) Refait, P.; Girault, P.; Jeannin, M.; Rose, J. Influence of arsenate species on the formation of Fe(III) oxyhydroxides and Fe(II-III) hydroxychloride. *Colloid. Surface. A* **2009**, *332*, 26−35.
(55) Riedel, T.; Zak, D.; Biester, H.; Dittmar, T. Iron traps terrestrially derived dissolved organic matter at redox interfaces. *Proc. Natl. Acad. Sci. U.S.A.* **2013**, *110*, 10101−10105.

(56) Borer, P.; Sulzberger, B.; Hug, S. J.; Kraemer, S. M.; Kretzschmar, R. Photoreductive dissolution of iron(III) (hydr)oxides in the absence and presence of organic ligands: Experimental studies and kinetic modeling. *Environ. Sci. Technol.* **2009**, *43*, 1864−1870.
(57) Mikutta, C.; Kretzschmar, R. Synthetic coprecipitates of exopolysaccharides and ferrihydrite. Part II: Siderophore-promoted dissolution. *Geochim. Cosmochim. Acta* **2008**, *72*, 1128−1142.
(58) Wan, M.; Shchukarev, A.; Lohmayer, R.; Planer-Friedrich, B.; Peiffer, S. Occurrence of surface polysulfides during the interaction between ferric (hydr)oxides and aqueous sulfide. *Environ. Sci. Technol.* **2014**, *48*, 5076−5084.
(59) Hellige, K.; Pollok, K.; Larese-Casanova, P.; Behrends, T.; Peiffer, S. Pathways of ferrous iron mineral formation upon sulfidation of lepidocrocite surfaces. *Geochim. Cosmochim. Acta* **2012**, *81*, 69−81.
(60) Hansel, C. M.; Benner, S. G.; Neiss, J.; Dohnalkova, A.; Kukkadapu, R. K.; et al. Secondary mineralization pathways induced by dissimilatory iron reduction of ferrihydrite under advective flow. *Geochim. Cosmochim. Acta* **2003**, *67*, 2977−2992.
(61) Wang, Y.; Morin, G.; Ona-Nguema, G.; Menguy, N.; Juillot, F.; et al. Arsenite sorption at the magnetite−water interface during aqueous precipitation of magnetite: EXAFS evidence for a new arsenite surface complex. *Geochim. Cosmochim. Acta* **2008**, *72*, 2573−86.
(62) Gallegos, T. J.; Han, Y.-S.; Hayes, K. F. Model predictions of realgar precipitation by reaction of As(III) with synthetic mackinawite under anoxic conditions. *Environ. Sci. Technol.* **2008**, *42*, 9338−9343.